M. Hernandez, A.M. Grande, S. Van Der Zwaag, S.J. Garcia
Monitoring Network and Interfacial Healing Processes by Broadband Dielectric Spectroscopy: a Case Study on Natural Rubber
ACS Applied Materials & Interfaces, Vol. 8, N. 16, 2016, p. 10647-10656
doi:10.1021/acsami.6b02259

"This is an Accepted Manuscript of an article published in ACS Applied Materials & Interfaces
2016, 8 (16), pp 10647–10656
available online: http://pubs.acs.org/doi/abs/10.1021/acsami.6b02259

Monitoring Network and Interfacial Healing Processes by Broadband Dielectric Spectroscopy: a Case Study on Natural Rubber

M. Hernández[1,*], A.M. Grande[1], S. van der Zwaag[1], S.J. García[1]

[1] *Novel Aerospace Materials Group, Faculty of Aerospace Engineering, Delft University of Technology, Kluyverweg 1, 2629 HS Delft, The Netherlands*

*corresponding author: m.hernandezsantana-1@tudelft.nl

ABSTRACT

Broadband dielectric spectroscopy (BDS) is introduced as a new and powerful technique to monitor network and macroscale damage healing in an elastomer. For the proof of concept a partially cured sulfur-cured natural rubber (NR) containing reversible disulfides as the healing moiety was employed. The forms of damage healed and monitored were an invisible damage in the rubber network due to multiple straining and an imposed macroscopic crack. The relaxation times of pristine, damaged and healed samples were determined and fitted to the Havriliak-Negami equation to obtain the characteristic polymer parameters. It is shown that seemingly full mechanical healing occurred regardless the type of damage, while BDS demonstrates that the polymer architecture in the healed material differs from that in the original one. These results represent a step forward in the understanding of damage and healing processes in intrinsic self-healing polymer systems with prospective applications such as coatings, tires, seals and gaskets.

Key words: broadband dielectric spectroscopy; polymer network healing; interfacial healing; natural rubber; intrinsic healing; disulfide

1. INTRODUCTION

Intrinsic self-healing polymers make use of reversible moieties to obtain on–demand or autonomous repair of macroscopic, microscopic or even molecular damages leading to the loss of certain functionality.[1] Since the emergence of the field of self-healing polymers several concepts using different reversible groups such as H-bonding, disulfides, Diels-Alder chemistry, and metalorganic ligands have attracted significant growing attention.[2-6] While self-healing repair is not intrinsically restricted to that of mechanical performance,[7] most of the published studies using intrinsic healing focus on the restoration of localized macroscale damages involving the creation of new interfaces (*e.g.* cracks or scratches) and the subsequent loss of stiffness and strength. Even though healing of macroscopic and optically detectable damage is important, the healing of

invisible internal damage (*i.e.* chain scission) to the polymer network is of equal importance. Hence techniques capable of determining the quality of the restoration of the polymer network either after macroscopic damage involving the creation of new interfaces or after (multi-cycle) straining not leading to any visible damage are crucial for the development of tailored self-healing materials having an extended lifetime.

Dielectric spectroscopy is a sensitive tool for probing multi-level molecular relaxations and has been used extensively to deepen our understanding of the structure-property relationships in polymers.[8-13] A broad dynamical range from 10^{-2} up to 10^{9} Hz can be covered and molecular motions taking place at extremely different time scales can be investigated with a single technique over a wide temperature domain. To do so, dielectric spectroscopy uses its sensitivity to molecular fluctuation of dipoles within the system which can be related to the molecular mobility of groups, segments or whole polymer chains which show up as different relaxation processes. Information on the structural state of the material can then be directly extracted by taking the molecular mobility spectrum as a probe for the structure.

In this study we use broadband dielectric spectroscopy (BDS) for the first time to follow the molecular dynamics evolution during healing of internal and macroscopic damage in a partially cured natural rubber (NR). Previous studies have shown that partially cured elastomers can undergo macroscopic healing by rearranging the rubber network without impairing the mechanical integrity.[14] In this work we do not focus on the quantification of the damage and healing as such by BDS, but demonstrate the use of this technique to monitor the molecular processes and the state of the material at the end of the healing treatment. To this aim both uniform molecular network damage (due to multiple straining cycles of the entire sample) and localized macroscopic damage (a macroscopic cut in an otherwise unstrained sample) were imposed and healed by suitable thermal treatments. The results obtained highlight the potential use of dielectric spectroscopy as a powerful technique for the development and understanding of intrinsic healing polymers.

2. EXPERIMENTAL

2.1. Materials

Natural rubber (NR) mainly consisting of *cis*-1,4-polyisoprene chains (*cis*-PI) was kindly supplied by *Wurfbain B.V.* under the trade name RSS3. The commercial grade ingredients employed as vulcanizing additives in the preparation of the NR compounds were used in the as-received state and are listed in Table 1.

Table 1. NR compound recipe.

Ingredient	Composition (phr)
NR	100
Zinc oxide (ZnO)	5
Stearic acid (SA)	1
N-cyclohexylbenzothiazole-2-sulphenamide (CBS)	0.14
Sulfur (S)	0.7

Sulfur cured NR compounds were prepared in an internal mixer (*Plasticorder 350S, Brabender*) according to the recipe given in Table 1. NR compound recipe.in parts per hundred of rubber (phr) in weight. A 2-step mixing protocol was followed: firstly, NR, ZnO and SA were mixed for 6 min; secondly, after 24 h, CBS and S were added and mixed for 4 min. Both mixing steps were done at 50 ^{o}C and 70 rpm.

2.2. Curing of rubber compounds

The rubber compounds were vulcanized in a laboratory compression press (*Wickert*) at 150 ^{o}C applying different curing times leading to 30% (t_{30}), 50% (t_{50}) and 90 % (t_{90}) of the maximum torque as derived from the corresponding curing curves obtained by means of a rubber process analyzer (*RPA2000, Alpha Technologies*) at T_c= 150 ^{o}C. Rectangular (70 x 10 mm) samples were cut out from 2 mm thick press-cured sheets, and circular (20 mm diameter) samples were cut out from films (~200 μm). All samples were subjected to damage, healing and dielectric spectroscopy tests. As-produced samples were defect-free.

2.3. Damage creation

2.3.1. Network damage

Molecular network damage was introduced to the rectangular samples by multiple (10) straining cycles at room temperature in a mechanical testing machine (*Zwick 1455*) to a maximum stretch ratio λ= 4 at a cross-head speed of 1 mm/s. The stretch ratio value selected was based on two premises: high enough to be close to the ultimate strain, but low enough so as to be on the limit of the strain induced crystallization of the rubber.[15, 16] The initial free length between the clamps was 40 mm. No visible damage was detectable after the cyclic deformation.

2.3.2. Macroscale interfacial damage

Macroscopic damage for broadband dielectric spectroscopy (BDS) measurements was introduced to the circular samples by creating a straight cut from the circumference of the disc to the disc center using a fresh scalpel blade. The cutting angle was perpendicular to the disc surface. The cut surface had a smooth and shiny surface.

Interfacial damage on samples to be evaluated by Single Edge Notched Tensile (SENT) test was also created for quantification of the healing efficiency. Specimens were stretched until failure and their Force-Displacement curves recorded. Fracture energy was then measured following a classical fracture mechanics approach.[17, 18] Details of the testing procedure are provided as Supporting Information S.1.

Important to mention that the 30%-cured samples were very difficult to handle due to their low curing degree. As a consequence it was not possible to gather information related to mechanical testing (either cyclic or fracture).

2.4. Healing procedure

2.4.1. Network healing

Healing of the cyclic strained rectangular samples not showing macroscale damage was done by pressure-less relaxation for 3 h at 70 ^{o}C in an oven. Healed samples were spectroscopically tested by BDS immediately after the healing treatment, as well as re-tested mechanically under the same initial loading conditions.

2.4.2. Macroscale healing

The cut circular samples were carefully positioned inside a home-built pressurized healing cell between two glass plates (see Figure 1) such that the cut surfaces were in seemingly optimal initial contact. The cut samples were subsequently healed under a controlled temperature (T= 70 ^{o}C) for a fixed time of 7 h while a constant pressure (P= 1 bar) was applied to the supporting glass plates. The application of a pressure on the glass plates and the resulting lateral expansion of sample assure the presence of a light contact pressure across the cut interface during healing. The selection of the healing conditions was based on previously reported results with other self-healing based on disulfides polymer systems.[3, 19, 20] During the healing treatment the morphology of the cut could be optically monitored. Healed samples were spectroscopically tested by BDS immediately after the healing treatment.

In order to mechanically quantify the healing efficiency, the two separated parts of the SENT samples were carefully repositioned together by hand and allowed to heal in the previously mentioned healing cell under the specified conditions. Healed SENT samples, equilibrated at RT for at least 30 minutes, were retested according to the same fracture protocol.

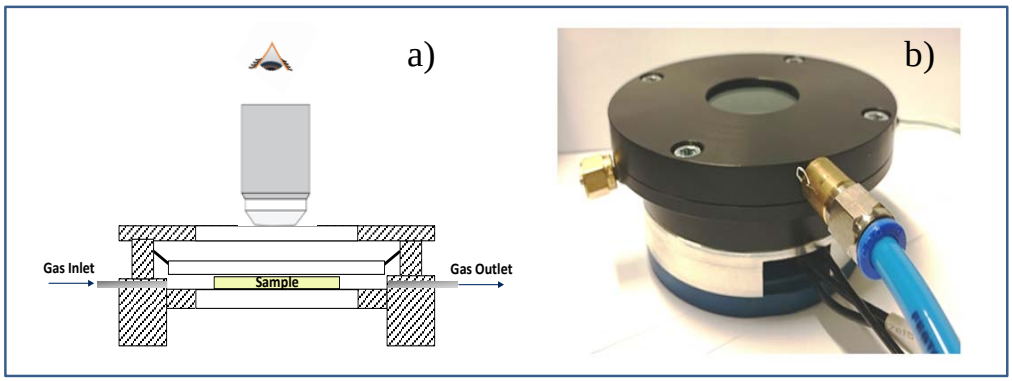

Figure 1. Home-built pressurized healing cell: a) cross-section; b) final set-up.

Table 2 summarizes the different samples that were damaged, healed and tested following comparable protocols.

Table 2. Damage and healing protocols.

Damage	Sample dimensions	Damage/healing measuring technique	Healing efficiency
Network damage (10 straining cycles)	Rectangular (70 x 10 x 2) mm	Mechanical testing	eq. (3)
Network damage (10 straining cycles)	Rectangular (70 x 10 x 2) mm	BDS	
Macroscale damage (SENT)	Rectangular (70 x 10 x 2) mm	Mechanical testing	eq. (6)
Macroscale damage (radial cut)	Circular d= 20 mm; t= 200 μm	BDS	

2.5. Material characterization

2.5.1. Crosslink density

The average mass of network chains between crosslinks (crosslink density, ν) was determined on the basis of solvent-swelling measurements in toluene by application of the Flory–Rehner equation[21] and assuming the formation of tetra-functional crosslinks during the vulcanization reaction.

2.5.2. Broadband dielectric spectroscopy (BDS)

BDS measurements were performed on an ALPHA high resolution dielectric analyzer (*Novocontrol Technologies GmbH*). All samples (pristine, damaged and healed) were mounted in the dielectric cell between two parallel gold-plated electrodes. The complex permittivity $\varepsilon^*(\omega) = \varepsilon'(\omega) - i\varepsilon''(\omega)$ of each sample was measured by performing consecutive isothermal frequency sweeps over a frequency window of $10^{-1} < f$ (Hz) $< 10^7$ (where $f=\omega/2\pi$ is the frequency of the

applied electric field being ω the angular frequency) in the temperature range from -100 to 100 ºC in steps of 5 ºC. The resulting relative error of each parameter is less than 3%.

The dielectric relaxation processes were analyzed quantitatively by fitting the frequency spectra to the Havriliak-Negami (HN) function[22-25] given by:

$$\varepsilon^*(\omega) = \varepsilon_\infty + \frac{\Delta\varepsilon}{[1+(i\omega\tau_{\mathrm{HN}})^b]^c} \quad (1)$$

The difference in dielectric constant measured at low and high frequencies is the *dielectric strength* (Δε) of the relaxation and it is related to the area under the absorption curve given by ($\Delta\varepsilon = \varepsilon_s - \varepsilon_\infty$), where ε_∞ and ε_s are the unrelaxed and relaxed values of the dielectric constant respectively. τ_{HN} is the HN relaxation time, representing the most probable relaxation time of the relaxation time distribution function,[26] and *b* and *c* are shape parameters ($0 < b, c \leq 1$) which describe the symmetric and the asymmetric broadening of the equivalent relaxation time distribution function, respectively. Parameters *b* and *c* can be associated to the structure and polymer architecture heterogeneity with respect to the bulk polymer.

The HN relaxation time τ_{HN} is related to the frequency of maximum loss, $f_{\max} = 1/(2\pi\tau_{\max})$, by the following equation:[27]

$$\tau_{\max} = \frac{1}{2\pi f_{\max}} = \tau_{\mathrm{HN}} \left(sin\frac{b\pi}{2+2c}\right)^{-1/b} \left(sin\frac{bc\pi}{2+2c}\right)^{1/b} \quad (2)$$

Both characteristic relaxation times coincide when the relaxation spectrum is symmetric, *i.e. c*=1.

3. RESULTS AND DISCUSSION

3.1. Monitoring of network damage healing

3.1.1. Mechanical testing analysis

Figure 2 shows representative stress-strain curves for 50%- and 90%-cured NR. For ease of visual comparison, only the first, second and the last (10^{th}) load cycles of the pristine and healed samples are shown. As seen in the figure, there is an important dependency of the mechanical properties on the degree of curing for pristine systems. While the 90% cured system shows a strain-hardening behavior (typically of fully cured NR), the 50% one exhibits a more liquid-like behavior suggesting lower amount of strong interchain covalent bonds formed between sulfur and the rubber backbone (disulfide bridges). The latter system is thus more prone to "flow" due to the higher mobility ensured by the lower amount of such bonds, although the overall mechanical behavior is also affected by physical entanglements.[28]

We also note that the stress-strain curves change differently from cycle to cycle for the two systems. The 50%-cured NR shows lower mechanical properties from the 2nd cycle onwards, lower mechanical properties being considered as lower value of the overall stress level and a lower Young's modulus as can be observed in Figure 2a). On the other hand, for the 90%-cured rubber it seems that the network is not drastically affected by the loading cycles since there is no substantial difference in the instantaneous modulus between all cycles (see Figure 2b). However, a small decrement in the maximum stress level is still observed. These aspects also reflect the observed hysteresis for the different systems. The 50% has a more viscoelastic behavior due to the minor chemical bonds amount and thus can dissipate more energy (large hysteresis) compared to the more "elastic" 90% cured system.

Regarding the healed systems, it also seems that the extent of mechanical recovery depends on the degree of curing. For both rubbers the instantaneous elastic modulus appears to be completely recovered in the first cycle (see Table 3), thus indicating apparent similar crosslinking densities between pristine and healed samples. However, the global tensile behavior differs after the thermal healing treatment. While for the 50%-cured NR similar curves are always obtained for the pristine and healed conditions (Figure 2a), the 90%-cured rubber shows higher discrepancy between the two curves at high strains (see inset in Figure 2b) as consequence of a softening effect, probably indicating a less healable system. This trend is understood as follows. For the 50%-cured NR, the potentially higher availability of reversible bonds leads to the recovery of the original properties. While for the 90%-cured rubber, the rupture of permanent bonds is irreversible, causing permanent damage.

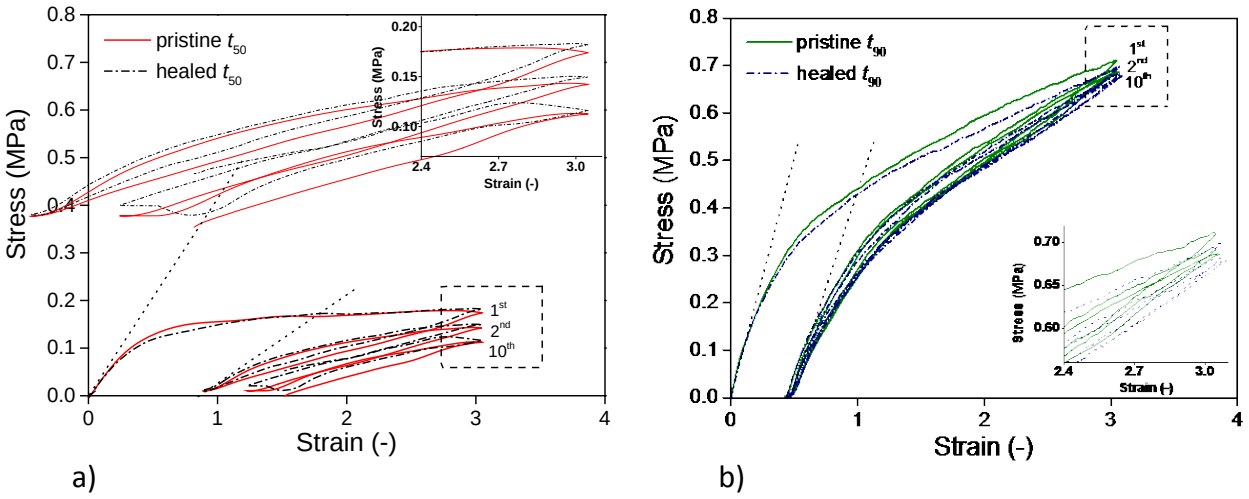

Figure 2. Stress-strain curves of NR samples under cyclic straining showing 1st, 2nd and 10th cycle: a) 50%-cured; b) 90%-cured. Insets correspond to end points of each cycle. Dotted lines have been included as guide to the eyes for better visualizing the instantaneous modulus variation between different loading cycles.

Since the instantaneous modulus is associated to irreversible and reversible chemical and physical constraints in the polymer network,[29] it is selected as the reference parameter for healing quantification according to the following equation:

$$\eta_{\text{bulk}} = \frac{\Delta E^{healed}}{\Delta E^{pristine}}\ x\ 100 \qquad (3)$$

where $\Delta E^{pristine}$ and ΔE^{healed} correspond to the difference in instantaneous tensile modulus between the 1st and 10th loading cycle for pristine and healed samples, respectively. Such an approach was selected in order to only consider the effect of reversible bonds on the recovery of mechanical properties since the residual permanent bonds (related to the instantaneous modulus of the 10th cycle) do not contribute to the network healing. Table 3 shows the calculated values. A higher recovery (96%) obtained for the 50%-cured NR reflects a larger amount of available reversible bonds in partially cured systems.

Table 3. Instantaneous moduli calculated numerically for the 1st and 10th loading cycle and healing efficiency values.

Compound	***E* (MPa)**				η_{bulk} **(%)**
	pristine (1st)	**pristine (10th)**	**healed (1st)**	**healed (10th)**	
t_{50}	0.49	0.22	0.48	0.22	96
t_{90}	1.25	0.86	1.14	0.89	64

Summarizing: less cured systems present lower mechanical performance, but higher damage when exposed to cyclic straining. However, such damage can be well repaired thanks to the overall mobility and reversibility of the sulfide bonds. On the contrary, fully cured systems show higher mechanical properties and smaller damage accumulation due to cycling, but lower healing efficiency due to the intrinsic irreversibility of such rubber network.

Having determined the mechanical characteristics and bulk healing ability of the developed NR compounds, the next section is devoted to understanding the molecular processes involved in the healing treatment by means of dielectric spectroscopy.

3.1.2. Broadband dielectric spectroscopy analysis

NR mainly consists of *cis*-PI chains with low polarity. Owing to the asymmetrical structure of *cis*-PI, NR has a dipole moment both parallel and perpendicular to the chain contour. Therefore, NR exhibits two relaxation modes.[9, 30, 31] At temperatures near the glass transition temperature (T_g= -64 ºC) the segmental mode, which is caused by the perpendicular component of the dipole and related to the segmental motions of the polymer chain, is observed and manifested as a maximum in the dielectric loss (ε'') spectrum. While at temperatures well beyond T_g, a more intense process due to the parallel component known as normal mode is also detected.

These two processes are affected when NR is vulcanized. On the one hand, vulcanizing by sulfur induces a slowing down of the segmental dynamics, leading to a shift of the position of the maximum in the dielectric spectrum to lower frequencies as the formation of sulfide crosslinks causes restrictions on the segmental motions of the polymer chains.[24, 32] It has also been found that the segmental dynamics of NR is not affected by the presence of entanglements or physical crosslinks.[11] While on the other hand, the normal mode disappears due to the crosslinking itself and to the suppression of large-scale motions of the dipole oriented parallel to the polymer backbone.[23] The effect of the damage and the healing steps on the segmental mode remaining after vulcanization is thus used in this study to analyze and understand healing by molecular dynamics.

To discuss the dependence of the dielectric loss (ε'') on frequency it is useful to consider its value normalized to its maximum value.[23] The un-normalized curves are presented as Supporting Information S.2. Figure 3 shows the normalized dielectric loss spectra of NR samples vulcanized for different curing times (t_{50} and t_{90}) over a wide frequency range and at a selected temperature (T= -40 ^{o}C) for pristine and after cyclic deformation damage and healed samples. This temperature is chosen since at this point, the segmental mode process is well centered and well resolved within the frequency window, and manifests itself as a relatively broad and asymmetric peak. Nevertheless, the trends obtained at this selected temperature can well be applied to the whole temperature range where the segmental mode is present. The temperature dependence of the segmental relaxation times derived from the Havriliak-Negami (HN) fitting will be addressed later in this section. Moreover, it can be seen how the molecular mobility of the polymer segments in the pristine samples is influenced by the crosslinking degree since the position of the maximum moves to lower frequencies (restricted dynamics) with increasing curing time due to the inherent constraints to the segmental motions imposed by the crosslinks (see Figure 3-a). The crosslink density values compiled in Table 4 further support this explanation.

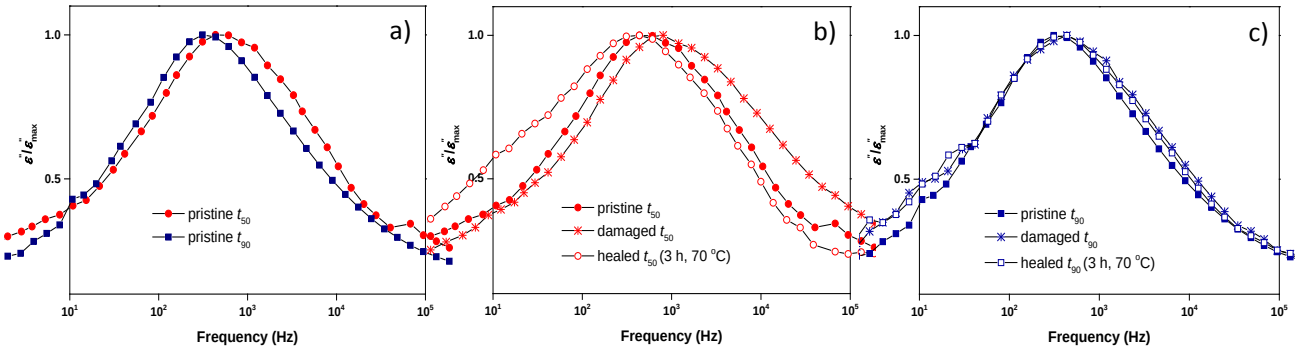

Figure 3. Normalized dielectric loss ε'' vs. frequency of NR samples in the region of the segmental mode at a selected temperature (T= -40 ^{o}C) for: a) pristine 50%- and 90%-cured; b) pristine, damaged and healed 50%-cured; c) pristine, damaged and healed 90%-cured.

Table 4. Crosslink density (ν) of pristine, damaged and healed samples, as a function of curing time.

Curing time (%)	Sample	Crosslink density, ν x10^4 (mol/g)
50	pristine t_{50}	2.53 ± 0.02
	damaged t_{50}	2.35 ± 0.02
	healed t_{50} (70 ^{o}C, 7 h)	2.54 ± 0.01
90	pristine t_{90}	2.70 ± 0.01
	damaged t_{90}	2.52 ± 0.03
	healed t_{90} (70 ^{o}C, 7 h)	2.61 ± 0.05

* t_{30} compounds were not measured due to partial dissolution of the samples

Two additional results can be extracted from Figure 3: *i*) the damaged samples show slightly faster dynamics, as follows from the shift of the position of the maximum of the dielectric loss to higher frequencies (Figure 3-b and-c), and *ii*) the loss spectra of the healed samples do not present any significant shift in frequency with respect to the pristine ones (Figure 3-b and -c). Such a behavior can be explained by the state of the polymer network after damage and after healing. When damaged, the rubber network undergoes chain scission, and so the chain dynamics are less hindered, being this effect more notorious for the 50%-cured sample. On the contrary, the healed NR shows a higher network constraint (slower dynamics) than the damaged which can be attributed to the reformation of bonds restricting and/or restoring the initial dynamics of the system. Again, crosslink density values compiled in Table 4 support these BDS interpretations.

Other interesting fact to discuss is the dissimilar broadening of the dielectric loss peak; towards high frequencies when damaged and towards low frequencies when healed (Figure 3-b). As previously stated, when damage takes place the crosslink density of the rubber compound decreases due to a partial destruction of the network. From a network dynamics point of view, and considering that the dielectric spectrum represents the average of all chain motions, it is thus expected that the damaged network spectrum should shift to high frequencies (less restricted motions) due to the increase of unconnected chains produced during scission.

On the contrary, the healing reaction involves not only changes in molecular mobility due to the reconnection of the chains, but also to some redistribution of the structure which leads to the formation of a new network with different architecture with respect to the pristine NR. In this case, the main contribution to the dynamics comes from larger scale motions (low frequencies) with increasing hindrance due to higher intermolecular interactions, while the higher dynamic events detected at high frequencies due to unconnected chains or dangling chains are reduced. These interpretations can be described by Schönhals and Schlosser[33] phenomenological model in which the shape of the dielectric loss peak is related to the behavior at low and high frequencies controlled by inter- and intra-molecular interactions, respectively.

In order to quantitatively analyze the changes, the relaxation parameters ($\Delta\varepsilon$, b, c and τ_{HN}) of each sample were calculated. Figure 4 shows the dielectric strength values for 50%- and 90%-cured pristine, damaged and healed NR in the temperature range of the segmental mode. An increase in

$\Delta\varepsilon$ with increasing curing time can be seen. In a first and rather simplified approach considering the system complexity, changes in $\Delta\varepsilon$ can be discussed based on the Frölich- Kirkwood (FK) equation:[24]

$$\Delta\varepsilon \propto \frac{4\pi\rho N_A}{9kTM} g\mu^2 \propto \mu_{eff}^2 \quad (4)$$

Where ρ is the density, μ is the dipole moment, M is the molecular weight of the repeating unit, N_A is the Avogadro´s number, k is the Boltzmann constant and g is the correlation factor which contains contributions of both inter and intra chain dipolar correlations and indicates the angular correlation between the dipole groups. The g factor is frequently referred to as a reduction factor since the term $g\mu^2$ corresponds to the effective dipole moment, μ_{eff}^2, of the material. The vulcanization reaction refers to the formation a crosslinked network of rubber chains. In sulfur vulcanizates, the following polar groups are reported to be present: (a) carbonyl groups; (b) mono- di- or polysulfide cross-links; (c) S-C bonds in the form of heterocyclic groups in the main chain.[24] Thus, it is expected than when the rubber is vulcanized the total number of polar groups involved would increase and consequently the dielectric strength as well as the restrictions in the rubber chains mobility would increase. It is important to mention that the other additives introduced in the rubber compound (stearic acid, zinc oxide, CBS) do not give any individual signal in the temperature/frequency range where the segmental relaxation of NR appear.

In sulfur-vulcanized NR as the crosslinking process continues from 50% to 90%, the fraction of sulfide bonds created between rubber chains increases. The increasing strength with curing can then be understood in terms of an increasing number of dipoles involved in the relaxation. The presence of di- and polysulfide crosslinks was confirmed by Raman and thiol-amine probe tests.[34] Disulfides are expected to give prominent Raman bands near 500 cm^{-1}, as confirmed from the spectra presented as Supporting Information S.3. Nonetheless, it is worth mentioning that the number of crosslinks compared to the total unsaturation level in NR is low, thus the variation on this band with curing time and with ageing is hard to quantify.

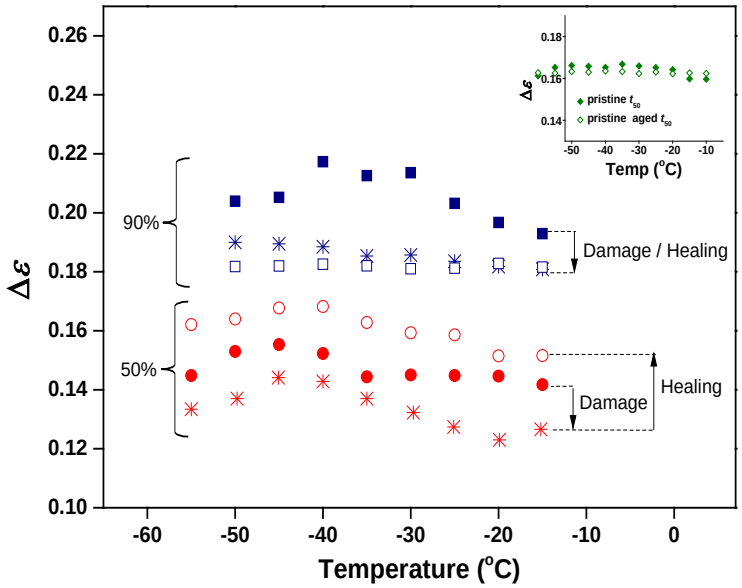

Figure 4. Dielectric strength $\Delta\varepsilon$ versus temperature for 50% and 90%-cured NR: pristine (solid symbols), cyclic damaged (star symbols) and healed (hollow symbols). Inset corresponds to pristine and pristine aged 50%-cured NR.

Figure 4 also shows that $\Delta\varepsilon$ decreases upon damage while it increases upon healing for the 50%-cured NR. Based on the previous statement, it could be argued that the increase observed for the healed 50%-cured NR reflects that further curing has taken place. Extra BDS tests on pristine (non-damaged) samples subjected to the same healing thermal treatment (70 ^{o}C, 7 h) were also done as control tests (pristine aged samples, see inset Figure 4). In BDS it is generally complex to accurately compare the signal strength $\Delta\varepsilon$ among different samples. This is because, for instance, inaccuracies in the sample thickness determination affect the signal. To overcome this problem and to facilitate the interpretations of the shifts and for being allowed to compare to other polymer systems, the difference of the dielectric strength of the pristine rubber to the dielectric strength of the damaged/healed ones was considered. Figure 5 shows the dielectric strength difference ($\Delta\Delta\boldsymbol{\varepsilon} = \Delta\boldsymbol{\varepsilon}_{\mathbf{pristine}} - \Delta\boldsymbol{\varepsilon}_{\mathbf{damaged/healed}}$) for the 50%- and 90%-cured NR accordingly, at a fixed temperature (T= -40 ^{o}C).

In Figure 5 it can be seen that a damaging event leads to a negative variation of $\Delta\Delta\varepsilon$ suggesting a decrease of the network polarization contradicting the expected result when pending groups are formed. Despite the fact that a direct relation cannot be fully explained based on the current results it may be that the dipolar contribution from the C-S bonds is partially cancelling out. On the contrary, with healing, small scale dipolar contributions seem to appear and so a positive variation is reflected on the chart. It should be realized that this is not the case for the 90%-cured sample. Seemingly, there is no complete recovery of the network when it is fully cured (no positive variation). Finally, the negligible $\Delta(\Delta\varepsilon)$ for the pristine aged samples suggests that no further crosslinking takes place under the selected thermal healing conditions.

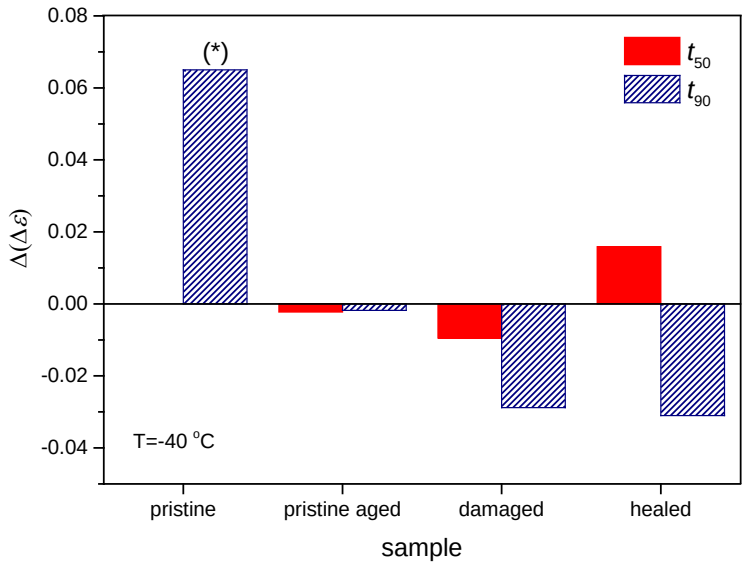

Figure 5. Dielectric strength difference $\Delta(\Delta\varepsilon)$ for 50%- and 90%-cured NR at T=-40 °C under different conditions: pristine, pristine aged, damaged, and healed. (*) Value calculated as $\Delta\Delta\boldsymbol{\varepsilon} = \Delta\boldsymbol{\varepsilon}_{\textbf{pristine 90\%}} - \Delta\boldsymbol{\varepsilon}_{\textbf{pristine 50\%}}$.

The temperature dependence of the segmental relaxation times (τ_{max}) was also studied. This dependency is well stated by the Vogel-Fulcher-Tammann (VFT) equation:[35-38]

$$\tau_{\max} = \tau_0 exp\left(\frac{B}{T-T_0}\right) \quad (5)$$

where τ_0 and B are temperature-independent parameters, and T_0 is the so-called ideal glass transition or Vogel temperature which is found to be 30-70 K below T_g.[39] To reduce the effect of misleading parameters on data fitting to the VFT equation over a limited frequency range, a value of $\tau_0 \approx 10^{-14}$ s was assumed, according to the values empirically found for many polymer systems lying between 10^{-14} and 10^{-12}.[8, 31, 40-42] The dependence of τ_{max} with temperature is depicted in Figure 6 and the VFT parameters listed in Table 5. This temperature dependency shows a clear curvature typical for cooperative motions. In this sense, all samples have comparable dynamics at high temperatures, whereas this behavior diverges at low temperatures, showing the 90%-cured NR the slowest dynamics. The curves for the pristine aged samples overlap with those of the pristine samples; indicating that the mild healing treatment does not lead to detectable further curing.

Calculated T_g values are also reported. By convention T_g is obtained by extrapolating the VFT fit to the temperature at which τ_{max} is equal to 100 s.[43] The calculated values are compatible with literature data validating the fitting.[28, 44] Although variations in T_g are within the range of experimental error, a slight reduction with damage due to the partial destruction of the network by chain scission and reduction in the segment length between cross-linking points would have been expected, while the reconnection of chains when healed would induce the recovery of T_g.

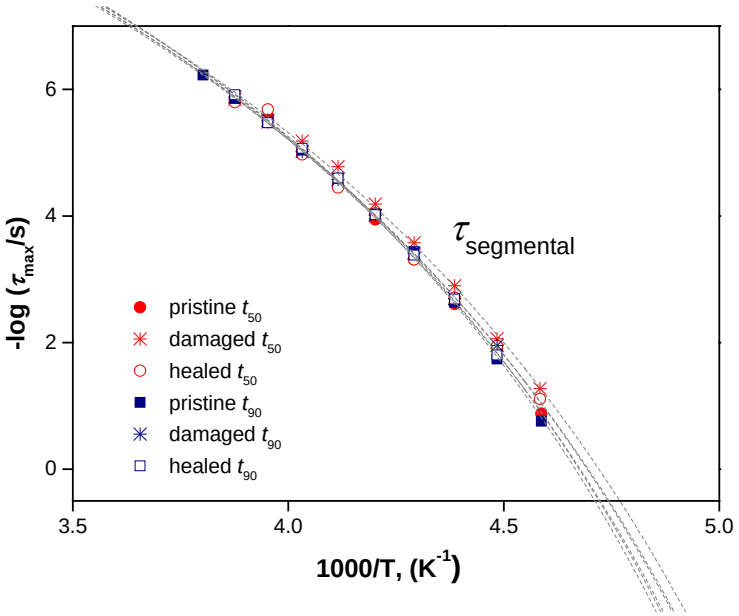

Figure 6. Temperature dependence of the average relaxation time for the segmental mode of pristine, cyclic damaged and healed NR samples vulcanized at different curing times. Dotted lines correspond to the VFT fit.

Table 5. VFT parameters and glass transition temperature (T_g) (calculated at τ_{max} = 100 s) of pristine, cyclic damaged and healed samples.

Compound	t_{50}			t_{90}		
	***B*(K)**	**T_0 (K)**	**T_g (^{o}C)**	***B***	**T_0(K)**	**T_g (^{o}C)**
pristine	2008	149	-69	1938	154	-66
damaged	2001	147	-71	2010	150	-68
healed	2015	150	-68	2007	150	-68

3.2. Monitoring of macroscale damage healing

3.2.1. Mechanical testing analysis

We also studied the healing of a macroscopic crack in both systems. A testing protocol based on fracture mechanics was used. It was recently demonstrated that such an approach provides more realistic measure of the interfacial healing achieved compared to tensile experiments.[18]

Results from fracture tests performed on pristine and healed samples are shown in Figure 7. The 50%-cured material has lower mechanical properties and potentially a higher healing capability compared to the 90%-cured NR. We quantified the mechanical recovery on SENT samples by:

$$\eta_{\text{fracture}} = \frac{G_c^{\text{healed}}}{G_c^{\text{pristine}}} x100 \qquad (6)$$

were G_c^{pristine} is the average fracture energy of the pristine SENT samples and G_c^{healed} is the average fracture energy for the healed ones. The 50%-cured grade showed a recovery of the fracture energy to 63%, while for the 90%-cured material this was only 36%. The difference in healing efficiency is clearly related to the number of reactive bonds available.

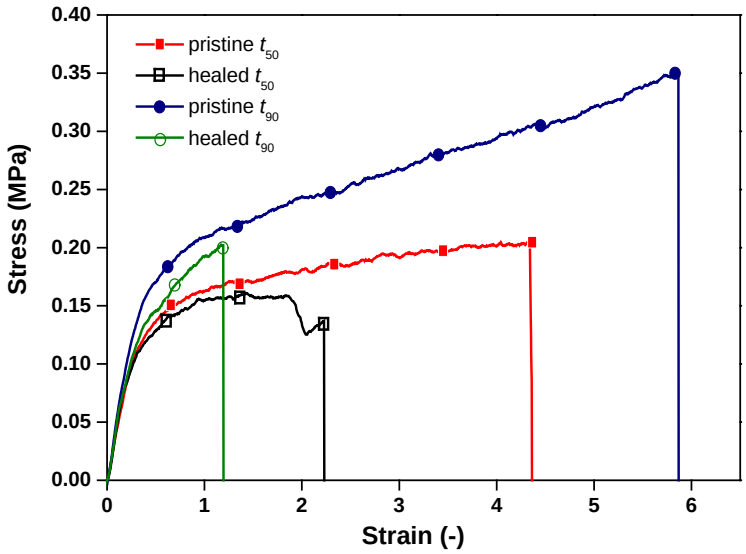

Figure 7. Stress-strain curves of pristine and healed SENT samples for different degrees of curing.

3.2.2. Broadband dielectric spectroscopy analysis

Figure 8 shows the normalized dielectric loss spectra of pristine and healed (7 h at T= 70 ^{o}C) NR samples vulcanized at different curing times (t_{30}, t_{50} and t_{90}). The samples cured at 30 and 50% showed interfacial healing with disappearance of the macroscale interface (see Figure 9) and retention of the mechanical integrity after tension (see Figure 7). A possible explanation to this behavior could be that interfacial diffusion of mobile rubber chains (adhesion of two surfaces) across the boundary faces has taken place. Nonetheless, the 90%-cured sample only showed partial interfacial healing and lower mechanical integrity retention, as stated in previous section. Such lack of sufficient interfacial healing for the 90%-cured NR made it impossible to measure its BDS spectrum. It is worth mentioning that this was also the case with all the as-damaged samples (contrary to those exposed to cyclic straining damage); the presence of air gaps between the two cut faces inhibited the completion of the BDS measurement already highlighting the potential of this technique for evaluating sufficient interfacial healing since only samples without macroscopic interfaces can be measured.

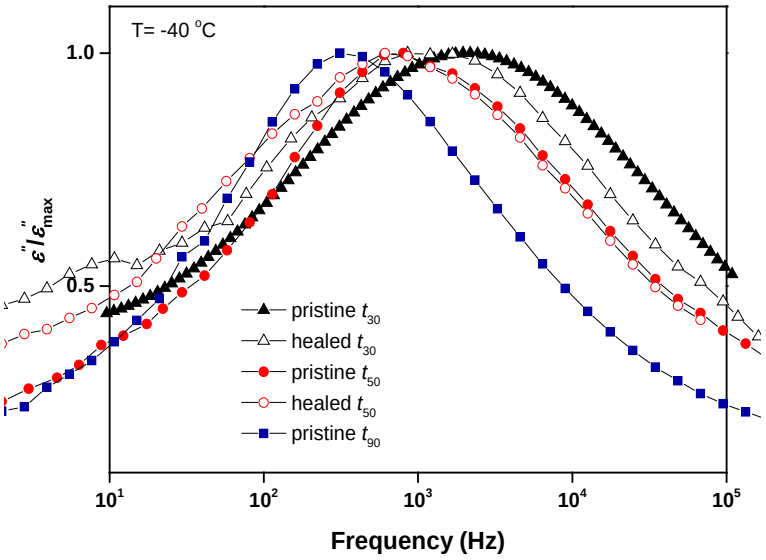

Figure 8. Normalized dielectric loss ε'' vs. frequency for the segmental mode (T= -40 °C) for pristine and healed NR samples vulcanized at different curing times. Filled symbols relate to pristine samples while hollow relate to healed ones.

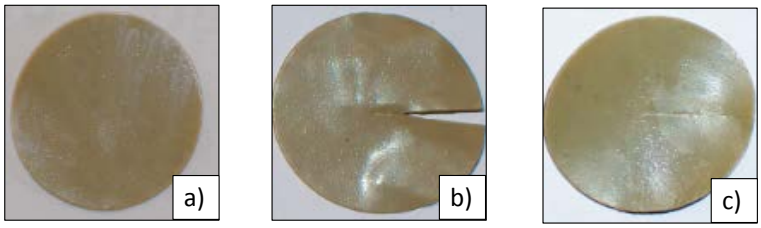

Figure 9. Photographs of a 50%-cured NR sample at different conditions: a) pristine; b) damaged; and c) healed.

The relaxation parameters ($\Delta\varepsilon$, b, c and τ_{HN}) of each compound were calculated and plotted. Figure 10 shows a representative set of relaxation curves and their fits (Figure 10-left) and fit parameters as a function of temperature (Figure 10-right) for the 50%-cured pristine and healed samples.

First of all, an increase in the dielectric strength $\Delta\varepsilon$ with healing is observed, as expected. Despite the reported changes may appear small, it should be noted that the $\Delta\Delta\varepsilon$ values for these macroscopic damaged samples are in the same order of magnitude (0.02-0.03) as those obtained for the network damaged samples (see Figure 5), giving reliability to the results. Also worth mentioning that samples with more than one cut (4 cuts in the center of the disk sample) were prepared. Results on such samples showed the same trend as that here (see Supporting Information S.4).

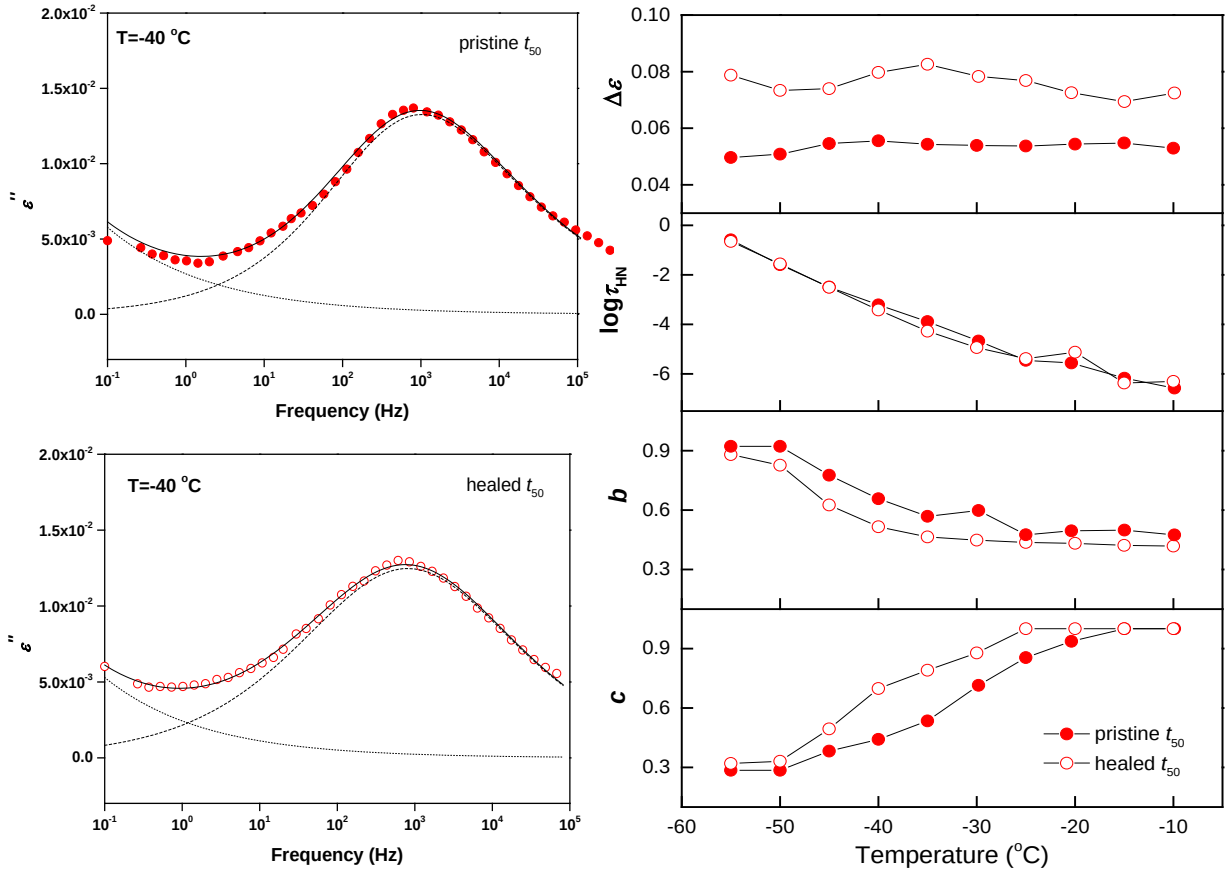

Figure 10. Left) Deconvolution results for the dielectric loss ε'' of pristine (top) and healed (bottom) 50%-cured NR samples. Solid lines represent the HN fitting curve, dashed lines the individual processes and dotted lines the conductivity contribution. Right) HN fitting parameters for the segmental mode of pristine and healed 50%-cured NR samples.

Secondly, with regard to the relationship between shape parameters (*b* and *c*) and the healing process, the general trend is that the ε'' curves presented in Figure 8 broaden (especially towards the low frequency side) as healing occurs. This broadening is expressed as a decrease in *b* value and an increase in *c* value tending to 1, as seen in Figure 8-right. The broadening and asymmetry of the segmental mode upon healing can be related to the presence of defects (*i.e.* network heterogeneities) due to differences in the polymer network architecture at the healing interface[1] despite the fact that optical observations suggest that the crack is fully healed. Based on this hypothesis, a molecularly 100% healed sample should show the same *b* and *c* values as the pristine, while a sample partially healed would show asymmetry, as in our case. Other examples of this heterogeneity (broadening) have be found when comparing the segmental mode of homopolymers and their corresponding copolymers[45] or blends.[46] The same effect is also observed when comparing the segmental mode of an amorphous polymer with its semi-crystalline peer.[47] In that case, the broadening is ascribed to the heterogeneity between the amorphous and semi-crystalline phases where the chain segments relax.

From the previous statements and having in mind that the $\Delta\varepsilon$, *b* and *c* parameters (*i.e.* width and shape) depend on structure of the chains or crosslink density, it becomes clear that the network structure at the interface has changed with the healing process. Nonetheless, if we consider that the τ_{HN} relaxation times do not vary with healing (Figure 10-right), it could be anticipated that the dynamics of the rubber compounds remained unaltered after healing. This fact can be confirmed by Figure 11.

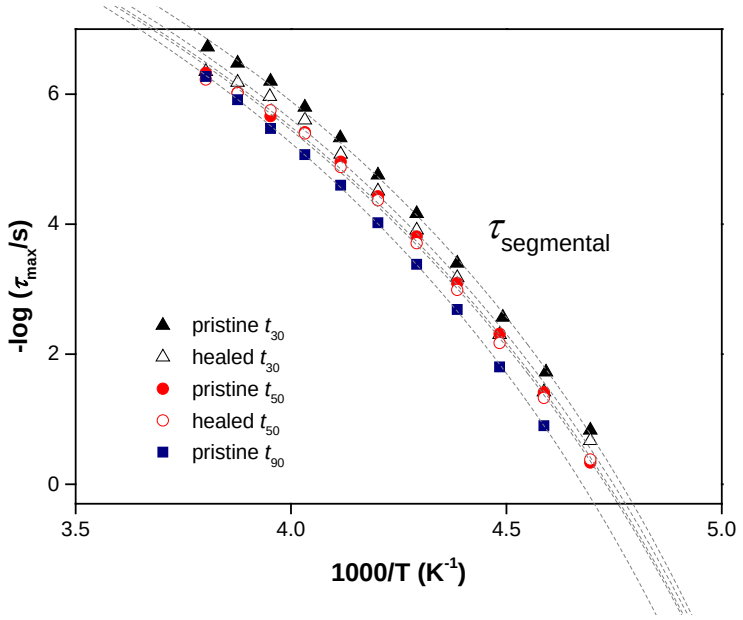

Figure 11. Temperature dependence of the average relaxation time for the segmental mode of pristine and healed NR samples vulcanized at different curing times. Dotted lines correspond to the VFT fit.

As it can be seen, τ_{max} gets bigger in the whole temperature range of the segmental mode as curing time increases, demonstrating a more restricted dynamics during the curing. Kramarenko *et al* examined the effect of crosslinking on the segmental dynamics in model polymer networks and concluded that the segmental motions above T_g experience growing hindrance and shift towards higher temperatures as the crosslinking density increases.[48] Therefore, the slowest segmental mode relaxation should be expected for the longer curing times (t_{90}). It is also clear that the relaxation times hardly vary with the healing process in the whole temperature range of the segmental mode for curing degrees up to 50%. Calculated T_g values listed in Table 6 confirm this statement. The negligible variation of T_g between pristine and healed samples points out the maintenance of high mobility of NR chains also after healing. It is also important to mention the similar calculated T_g values (Table 5 vs. Table 6), reflecting the consistency of the technique and the independence on sample geometry.

Table 6. Glass transition temperature (T_g) of pristine and healed samples vulcanized at different curing times, calculated from BDS measurements at τ_{max} = 100 s.

Compound	T_g (°C)	
	pristine	healed
t_{30}	-70	-70
t_{50}	-69	-69
t_{90}	-66	---*

*not measured

4. CONCLUDING STATEMENTS

The potential of broadband dielectric spectroscopy, with its unique ability to describe mobility as a function of polymer architecture, has been explored and used as a powerful tool to assess macroscale and network polymer healing processes. The dynamic relaxations analysis of sulfur-cured NR compounds gives evidence on the formation of a heterogeneous network structure at the healed interface or in the bulk after the partial recovery of the macroscale damaged interface and/or strained polymer network. The crosslink density seems to be the limiting factor for the relatively slow healing kinetics of the studied systems. A good correlation has been found between crosslinking density, T_g and healing efficiency, when monitoring the healing process at a scale close to the relevant molecular processes. This proof of concept and findings are quite remarkable and represent a step forward in the understanding of the formation of new heterogeneous networks during the healing process, especially during the restoration of macroscopic damages. Further tests with different polymer networks will give more light to the potential of BDS to analyze and quantify the degree of interfacial and bulk healing based on the dynamics and on the level of heterogeneity formed during damage-healing.

ASSOCIATED CONTENT

Fracture test protocol for the determination of the fracture energy G_c is supplied as Supporting Information S.1. Un-normalized dielectric spectra of NR samples with different curing times are supplied as Supporting Information S.2. Raman measurements of NR samples with different curing times are supplied as Supporting Information S.3. HN parameters for 50%-cured NR samples with multiple damage cuts are supplied as Supporting Information S.4.

ACKNOWLEDGEMENTS

M. Hernández thanks the European Commission for a Marie Curie Fellowship (PIEF-GA-2013-623379). A. Grande thanks a funding via the SHINE project (EU 309450-2). The authors also acknowledge the Elastomer Technology and Engineering group (Dr. W. Dierkes and Miss. K. Sengloyluan) from University of Twente for their support in the preparation of the rubber compounds.

REFERENCES

1. Garcia, S. J., Effect of Polymer Architecture on the Intrinsic Self-Healing Character of Polymers. Eur. Polym. J. **2014**, 53, 118-125.

2. Cordier, P.; Tournilhac, F.; Soulie-Ziakovic, C.; Leibler, L., Self-Healing and Thermoreversible Rubber from Supramolecular Assembly. Nature **2008**, 451 (7181), 977-980.

3. Canadell, J.; Goossens, H.; Klumperman, B., Self-Healing Materials Based on Disulfide Links. Macromolecules **2011**, 44 (8), 2536-2541.

4. Herbst, F.; Seiffert, S.; Binder, W. H., Dynamic Supramolecular Poly(Isobutylene)S for Self-Healing Materials. Polym. Chem. **2012**, 3 (11), 3084-3092.

5. Hager, M. D.; Greil, P.; Leyens, C.; van der Zwaag, S.; Schubert, U. S., Self-Healing Materials. Adv. Mater. **2010**, 22 (47), 5424-5430.

6. Sandmann, B.; Bode, S.; Hager, M. D.; Schubert, U. S., Metallopolymers as an Emerging Class of Self-Healing Materials. In *Hierarchical Macromolecular Structures: 60 Years after the Staudinger Nobel Prize Ii*, Percec, V., Ed. 2013; Vol. 262, pp 239-257.

7. Garcia, S. J.; Fischer, H. R.; van der Zwaag, S., A Critical Appraisal of the Potential of Self Healing Polymeric Coatings. Prog. Org. Coat. **2011**, 72 (3), 211-221.

8. Mijovic, J.; Lee, H. K.; Kenny, J.; Mays, J., Dynamics in Polymer-Silicate Nanocomposites as Studied by Dielectric Relaxation Spectroscopy and Dynamic Mechanical Spectroscopy. Macromolecules **2006**, 39 (6), 2172-2182.

9. Hernández, M.; Carretero-Gonzalez, J.; Verdejo, R.; Ezquerra, T. A.; López-Manchado, M. A., Molecular Dynamics of Natural Rubber/Layered Silicate Nanocomposites as Studied by Dielectric Relaxation Spectroscopy. Macromolecules **2010**, 43 (2), 643-651.

10. Linares, A.; Nogales, A.; Sanz, A.; Ezquerra, T. A.; Pieruccini, M., Restricted Dynamics in Oriented Semicrystalline Polymers: Poly(Vinilydene Fluoride). Physical Review E **2010**, 82 (3), 031802.

11. Carretero-Gonzalez, J.; Ezquerra, T. A.; Amnuaypornsri, S.; Toki, S.; Verdejo, R.; Sanz, A.; Sakdapipanich, J.; Hsiao, B. S.; Lopez-Manchado, M. A., Molecular Dynamics of Natural Rubber as Revealed by Dielectric Spectroscopy: The Role of Natural Cross-Linking. Soft Matter **2010**, 6 (15), 3636-3642.

12. Hernández, M.; Ezquerra, T. A.; Verdejo, R.; López-Manchado, M. A., Role of Vulcanizing Additives on the Segmental Dynamics of Natural Rubber. Macromolecules **2012**, 45 (2), 1070-1075.

13. Martin-Fabiani, I.; Linares, A.; Nogales, A.; Ezquerra, T. A., Dielectric Relaxation of Poly (Trimethylene Terephthalate) in a Broad Range of Crystallinity. Polymer **2013**, 54 (21), 5892-5898.

14. Gent, A. N.; Lai, S. M., Interfacial Bonding, Energy-Dissipation, and Adhesion. J. Polym. Sci., Part B: Polym. Phys. **1994**, 32 (8), 1543-1555.

15. Toki, S.; Hsiao, B. S.; Amnuaypornsri, S.; Sakdapipanich, J., New Insights into the Relationship between Network Structure and Strain-Induced Crystallization in Un-Vulcanized and Vulcanized Natural Rubber by Synchrotron X-Ray Diffraction. Polymer **2009**, 50 (9), 2142-2148.

16. Hernández, M.; López-Manchado, M. A.; Sanz, A.; Nogales, A.; Ezquerra, T. A., Effects of Strain-Induced Crystallization on the Segmental Dynamics of Vulcanized Natural Rubber. Macromolecules **2011**, 44 (16), 6574-6580.

17. Greensmith, H. W., Rupture of Rubber. X. The Change in Stored Energy on Making a Small Cut in a Test Piece Held in Simple Extension. J. Appl. Polym. Sci. **1963**, 7 (3), 993-1002.

18. Grande, A. M.; Garcia, S. J.; van der Zwaag, S., On the Interfacial Healing of a Supramolecular Elastomer. Polymer **2015**, 56, 435-442.

19. AbdolahZadeh, M.; Esteves, A. C. C.; van der Zwaag, S.; Garcia, S. J., Healable Dual Organic-Inorganic Crosslinked Sol-Gel Based Polymers: Crosslinking Density and Tetrasulfide Content Effect. J. Polym. Sci., Part A: Polym. Chem. **2014**, 52 (14), 1953-1961.

20. Pepels, M.; Filot, I.; Klumperman, B.; Goossens, H., Self-Healing Systems Based on Disulfide-Thiol Exchange Reactions. Polym. Chem. **2013**, 4 (18), 4955-4965.

21. Flory, P. J.; Rehner, J., Statistical Mechanics of Cross-Linked Polymer Networks Ii Swelling. J. Chem. Phys. **1943**, 11 (11), 521-526.

22. Havriliak.S; Negami, S., A Complex Plane Representation of Dielectric and Mechanical Relaxation Processes in Some Polymers. Polymer **1967**, 8 (4), 161-210.

23. Kremer, F.; Schönhals, A., Broadband Dielectric Spectroscopy. Springer: New York, 2003; p 721.

24. Hedvig, P., Dielectric Spectroscopy of Polymers. Bristol, 1977.

25. Debye, P., Polar Molecules. Dover Publications: New York, 1945.

26. Böttcher, C. J. F.; Bordewijk, P., Theory of Electric Polarization. Elsevier: 1978; Vol. II.

27. Richert, R.; Angell, C. A., Dynamics of Glass-Forming Liquids. V. On the Link between Molecular Dynamics and Configurational Entropy. J. Chem. Phys. **1998**, 108 (21), 9016-9026.

28. Brydson, J. A., Rubbery Materials and Their Compounds. Elsevier Science Publishers Ltd: London, 1988; p 469.

29. Rubinstein, M.; Panyukov, S., Elasticity of Polymer Networks. Macromolecules **2002**, 35 (17), 6670-6686.

30. Adachi, K.; Kotaka, T., Dielectric Normal-Mode Relaxation. Prog. Polym. Sci. **1993**, 18 (3), 585-622.

31. Cerveny, S.; Zinck, P.; Terrier, M.; Arrese-Igor, S.; Alegria, A.; Colmenero, J., Dynamics of Amorphous and Semicrystalline 1,4-Trans-Poly(Isoprene) by Dielectric Spectroscopy. Macromolecules **2008**, 41 (22), 8669-8676.

32. Hernandez, M.; Valentin, J. L.; Lopez-Manchado, M. A.; Ezquerra, T. A., Influence of the Vulcanization System on the Dynamics and Structure of Natural Rubber: Comparative Study by Means of Broadband Dielectric Spectroscopy and Solid-State Nmr Spectroscopy. Eur. Polym. J. **2015**, 68, 90-103.

33. Schonhals, A.; Schlosser, E., Dielectric-Relaxation in Polymeric Solids .1. A New Model for the Interpretation of the Shape of the Dielectric-Relaxation Function. Colloid. Polym. Sci. **1989**, 267 (2), 125-132.

34. Campbell, D. S., Structural Characterization of Vulcanizates .10. Thiol-Disulfide Interchange for Cleaving Disulfide Crosslinks in Natural Rubber Vulcanizates. J. Appl. Polym. Sci. **1969**, 13 (6), 1201-1214.

35. Fulcher, G. S., Analysis of Recent Measurements of the Viscosity of Glasses. J. Am. Ceram. Soc. **1925**, 8 (6), 339-355.

36. Vogel, H., The Temperature Dependence Law of the Viscosity of Fluids. Physikalische Zeitschrift **1921**, 22, 645-646.

37. Tammann, G.; Hesse, W., The Dependancy of Viscosity on Temperature in Hypothermic Liquids. Zeitschrift Fur Anorganische Und Allgemeine Chemie **1926**, 156 (4).

38. Bohmer, R.; Ngai, K. L.; Angell, C. A.; Plazek, D. J., Nonexponential Relaxations in Strong and Fragile Glass Formers. J. Chem. Phys. **1993**, 99 (5), 4201-4209.

39. Fischer, E. W., Light-Scattering and Dielectric Studies on Glass-Forming Liquids. Physica A **1993**, 201 (1-3), 183-206.

40. Fritzsche, J.; Das, A.; Jurk, R.; Stoeckelhuber, K. W.; Heinrich, G.; Klueppel, M., Relaxation Dynamics of Carboxylated Nitrile Rubber Filled with Organomodified Nanoclay. Express Polym. Lett. **2008**, 2 (5), 373-381.

41. Mok, M. M.; Masser, K. A.; Runt, J.; Torkelson, J. M., Dielectric Relaxation Spectroscopy of Gradient Copolymers and Block Copolymers: Comparison of Breadths in Relaxation Time for Systems With. Increasing Interphase. Macromolecules **2010**, 43 (13), 5740-5748.

42. Hayakawa, T.; Adachi, K., Dielectric Relaxation of Poly(N-Butyl Acrylate). Polym. J. **2000**, 32 (10), 845-848.

43. Angell, C. A., Relaxation in Liquids, Polymers and Plastic Crystals - Strong Fragile Patterns and Problems. J. Non·Cryst. Solids **1991**, 131, 13-31.

44. Roberts, A. D., Natural Rubber Science and Technology. Oxford University Press: Oxford, 1988; p 1136.

45. Santangelo, P. G.; Ngai, K. L.; Roland, C. M., Temperature Dependence of Relaxation in Polypropylene and Poly(Ethylene-Co-Propylene). Macromolecules **1996**, 29 (10), 3651-3653.

46. Zetsche, A.; Kremer, F.; Jung, W.; Schulze, H., Dielectric Study on the Miscibility of Binary Polymer Blends. Polymer **1990**, 31 (10), 1883-1887.

47. Sanz, A.; Nogales, A.; Ezquerra, T. A.; Haussler, W.; Soccio, M.; Lotti, N.; Munari, A., Homogeneous Dynamics within Inhomogeneous Environment in Semicrystalline Polymers. Macromolecules **2011**, 44 (20), 8124-8128.

48. Kramarenko, V. Y.; Ezquerra, T. A.; Sics, I.; Balta-Calleja, F. J.; Privalko, V. P., Influence of Cross-Linking on the Segmental Dynamics in Model Polymer Networks. J. Chem. Phys. **2000**, 113 (1), 447-452.

TABLE OF CONTENTS

Monitoring Network and Interfacial Healing Processes by Broadband Dielectric Spectroscopy: a Case Study on Natural Rubber

M. Hernández, A.M. Grande, S van der Zwaag and S.J. García